Applied Catalysis B: Environmental 182 (2016) 15–25

Contents lists available at ScienceDirect

Applied Catalysis B: Environmental

journal homepage: www.elsevier.com/locate/apcatb

A new approach to polymer-supported phosphotungstic acid: Application for glycerol acetylation using robust sustainable acidic heterogeneous–homogenous catalyst

M.A. Betiha[a,*], Hassan M.A. Hassan[b,**], E.A. El-Sharkawy[b], A.M. Al-Sabagh[a], M.F. Menoufy[a], H-E.M. Abdelmoniem[b]

[a] Egyptian Petroleum Research Institute, Cairo, 11727 Naser City, Egypt
[b] Department of Chemistry, Faculty of Science, Suez University, Suez, Egypt

ARTICLE INFO

Article history:
Received 2 July 2015
Received in revised form 2 September 2015
Accepted 5 September 2015
Available online 8 September 2015

Keywords:
Renewable energy
Glycerol acetylation
Porous polymer
Heterogeneous catalyst
Phosphotungstic acid functionalization

ABSTRACT

Biodiesels produced from renewable sources is now recognized as a green fuel and exhibit superior fuel properties, and they are more environmentally friendly than petroleum-based fuels. In this paper, the functionalization was performed through quaternization of one amine belonged ethylenediamine with chloromethyl group of solid polymer, and the remaining amine could act as active sites to immobilize $H_3PW_{12}O_{40}$ (PTA) through ionic bonding interaction. Thanks to the strong acidity of PTA and swelling behavior of ethylenediamine on the surface and micro-mesochannels of poly(divinylbenzene-co-vinylbenzyl chloride) copolymer (PDVC), the catalysts showed properties of heterogeneous and homogeneous behavior and presents new opportunities for tailored new solid acids in sustainable chemistry. The catalysts were characterized by various structural morphology (XRD, N_2- sorption, HRTEM and FESEM) and compositional (FTIR, Raman spectra and XPS) techniques.

This catalyst showed much higher activity than other solid acidic catalysts due to the enriched PTA-surface acid sites (6.78 mmol g^{-1}) and the minimized diffusion limitation as well as high level of catalyst dispersion in reaction mixture due to the unique structure. Furthermore, by enclosing the PTA acidic material to a tailored free amino group in PDVC, an even more enduring catalyst was developed and applied to glycerol acetylation reaction. This catalyst displayed high conversion (99.9%), selectivity toward triacetin (73%) and superior performance in terms of endurance and leaching control of active sites compared with other catalysts. The catalyst was capable of withstanding for seven times durable run of continuous process at 100 °C without deactivation. During the reaction time, the leaching of PTA species was not observed and the material maintained its structural integrity.

1. Introduction

The development of modern technologies for producing chemicals and green energy from sustainable resources has been quickly prompting throughout the world as a possible substitute for the petroleum based fuels because it is renewable, biodegradable, and biocompatible new energy sources [1]. Wide spread commercialization of biodiesel has in turn led to dissipate an oversupply of crude glycerol in the market as a byproduct until new technologies are created for glycerol by way of new product development. Glycerol is the main by-product in transesterification reaction of oil or waste oil with alcohols like methanol or ethanol. Since glycerol is functionalized molecule with three hydroxyl groups, it is considered as a potential renewable feedstock for numerous valuable products [2,3]. Glycerol can undergo oxidation, hydrogenolysis [4,5], carbonylation [6–8], esterification and etherification [9], etc., to yield useful commodity chemicals.

One of the important reactions is synthesis of acetin from esterification of glycerol with acetic acid, which are known valuable chemicals and fuel additives. In addition, the acetylated glycerol derivatives (monoacetain, MAG, diacetain (DAG), and triacetain (TAG)) have gained more attention to find better utilization of surplus glycerol resulted from the biodiesel transesterification processes. MAG is used in manufacturing of explosives and tanning agent as solvent for dyes. DAG is used as a solvent, plasticizer and

* Corresponding author. Fax: +20 222747433.
** Corresponding author. Fax. +20 2 050 2246781.
E-mail addresses: Mohamed_betiha@yahoo.com (M.A. Betiha), hmohamed_73@yahoo.com (H.M.A. Hassan).

http://dx.doi.org/10.1016/j.apcatb.2015.09.010
0926-3373/

softening agent. TAG is used as a solvent for diluting drugs and organic compounds. Furthermore, valorization of glycerol derivatives (DAG and TAG) as fuel additives can not only improving properties of diesel fuel by enhancing pour point, flash point and viscosity but also reduce particulate emissions and the cost of biofuel [3,10].

The MAG, DAG and TAG can be catalytically formed by acetylation of glycerol with acetic acid or acetic anhydride with heterogeneous or homogeneous catalysts. Homogeneous acid catalysts such as *p*-toluene sulfonic acid, H_3PO_4 and HCl have been used for the glycerol acetylation. However, homogeneous catalysts cause several problems, including corrosion of the reactor, production of several toxic compounds and catalysts loss due to the difficulty of separation. To overcome these drawbacks, research interest has been mainly forced to discover eco-friendly and highly active heterogeneous catalysts, such as acid or base solid catalysts. In the last few years, several studies were reported by using varies solid acid catalysts such as Amberlyst-15, acidic mesoporous silica, sulfonated-carbon and dodecatungstophosphoric acid immobilized onto a silica for glycerol acetylation from reaction of glycerol with acetic acid [10–14]. Amberlyst-15 acid resin showed a conversion of 90% and selectivities of 54% and 13% toward DAG and TAG, respectively, after 10 min at 150 °C [11]. However, the main drawback of the Amberlyst-15 is its low thermal stability, which leads to corrosion problems caused by its decomposition, and therefore inhibits the possibility of regeneration [12]. Sulfonic acid functionalized mesostructured materials catalyst showed 90% of glycerol conversion with combined selectivity toward DAG and TAG of 85% at 125 °C after 4 h [10]. SO_3H-carbon catalyst gave glycerol conversion (91%) and selectivities of 38% (MAG), 28% (DAG) and 34% (TAG) at reaction condition of 120 °C and 3 h of reaction time [13]. Silica supported dodecatungstophosphoric acid catalyst achieved 62% (DAG) and 3% (TAG) selectivities [14].

Supported heteropoly acids (HPAs), especially 12-tungstophosphoric acid (PTA), have become widespread materials to catalyze a wide variety of reactions because of their unique properties such as redox natures, super acidic properties (strong Brønsted acids) and the keggin structure, and can be used in homogeneous as well as heterogeneous catalysis [15–17]. However, HPA has several shortcomings such as thermal instability, low surface area (<10 m^2/g), aggregating easily and separation problem from reaction mixtures. These problems can overcome by loading HPAs on the different supporters of stable structure and high surface area. Supported PTA has also been used for performing glycerol esterification reaction [18–20]. PTA supported on Cs-containing zirconia [18], activated carbon [14], cubic mesoporous silica [19] and niobic acid [20] have been reported for glycerol esterification. The disadvantages of these acidic solid catalysts such as limitation of pore-size, reuse and low selectivity toward the favored DAG and TAG materials are still unresolved issues for industrial applications due to leaching of PTA from the supports.

Despite the many investigations, the need for a supper acidic solid catalysts for glycerol upgrading and development of green technologies to obtain sustainable energy and valuable chemicals on their basis still exists. With these considerations in mind, we have tried to develop high acidic solid catalysts that are easy to prepare, cost-effective and free active sites leaching. In the present work, the authors report the synthesis of crosslinked polymer tailored inorganic acid through soft crosslinking agent as ethylenediamine. One amine of ethylenediamine could be quaternized with chloromethyl group belong to solid polymer and the remaining amine functional group could act as active sites to immobilize $H_3PW_{12}O_{40}$ (PTA). In this way, both sintering and leaching of the PTA is eliminated and the properties for supporting active species are preserved. In addition, this study in particular investigates the influence of acidic properties, catalyst structure and reaction parameters on triacetin formation, and compares the results with other commercial catalysts. Further, to our best knowledge this is also the first account showcasing the application of PTA-polymer as stable recyclable catalysts for glycerol acetylation with high selectivity toward triacetin formation than others.

2. Experimental

2.1. Materials

P-divinylbenzene (DVB, 85%), 4-vinylbenzyl chloride (VBC, 90%), cetrimonium bromide (CTAB, ≥99%), Benzoyl peroxide (BOP, 75%), ethylenediamine (ED, ≥99%), anhydrous 12-tungstophosphoric acid (PTA, 99.995%), neutral red (Dye content ≥90 %), glycerol (Gly, ≥99.5%), acetic acid (AA, ≥99.7%), potassium hydroxide (90%) and phenolphthalein were purchased from Sigma-Aldrich. The contents of DVB stabilizer was removed by several washing with a 1N NaOH solution followed by drying under sodium sulfate. BOP was purified by recrystallization from hot chloroform. 1, 2-dichloroethane (DCE), diethyl ether (DEE), tetrahydrofuran (THF), methanol and ethanol were purchased from Adwic (Egypt) and used after distillation and drying over an A4 molecular sieve directly before use.

2.2. Synthesis of monolithic poly(DVB-co-VBC) copolymer (PDVC)

The PDVC beads were prepared by emulsion polymerization. Aqueous solutions of 1.5 g of CTAB in 45.50 mL of water (warmed until the CTAB dissolved), 15.0 g (98.28 mmol) of VBC, 12.79 g (98.28 mmol) of DVB and 0.283 g (1.17 mmol) of BOP were charged into a 150 mL round-bottom flask fitted with a condenser, N_2 gas inlet and thermometer. The mixture was bubbled for 30 min with nitrogen gas to remove dissolved oxygen. The flask was heated to 80 °C over a 30 min period under stirring speed of 500 rpm, and then the temperature decreased to 60 °C for 24 h. The yellowish precipitate was filtered off, washed with water/methanol several times, followed by Soxhlet extraction with toluene and finally washed with diethyl ether/methanol mixture.

2.3. Synthesis of aminated monolithic poly(DVB-co-VBC) copolymer (H_2N-PDVC)

In a three-necked round flask (100 mL), the resulting monolithic PDVC (5.0 g, 17.76 mmol of chloromethyl groups) was stirred in 50 mL toluene for 1 h under N_2 gas flow, and ED (53.03 mmol; molar ratio of amine/chloromethyl groups 3/1) in 30 mL toluene was added at 0 °C for 2 h. The temperature was raised gradually to 60 °C for 3 h and the product was filtered off, washed with H_2O/MeOH (1:2) and EtOH to remove unreacted ED material. The product was dried under vacuum at 20 °C over night.

2.4. Synthesis of PTA-H_2N-PDVC (Cat-A, Cat-B and Cat-C)

The impregnation method derived PTA-H_2N-PDVC-x catalysts was synthesized as follows: *x* g (*x* = 5.9, 3.94 and 1.96 g; 2.05, 1.36 and 0.68 mmol, respectively) of PTA was dissolved in 50 mL of distilled water/THF mixture (80:20; V/V). Then, 0.58 g (2.05 mmol) of H_2N-PDVC was directly added to the solution at 60 °C under vigorous stirring for 8 h. The excess water/THF mixture was evaporated at 60 °C under depressed pressure, and the obtained solid was washed with distilled water several times to remove excess PTA and air dried at 40 °C for 12 h. The catalysts are denoted as Cat-A, Cat-B and Cat-C where A, B and C characters represented the molar ratio of PTA and aminated chloromethyl groups, Scheme 1.

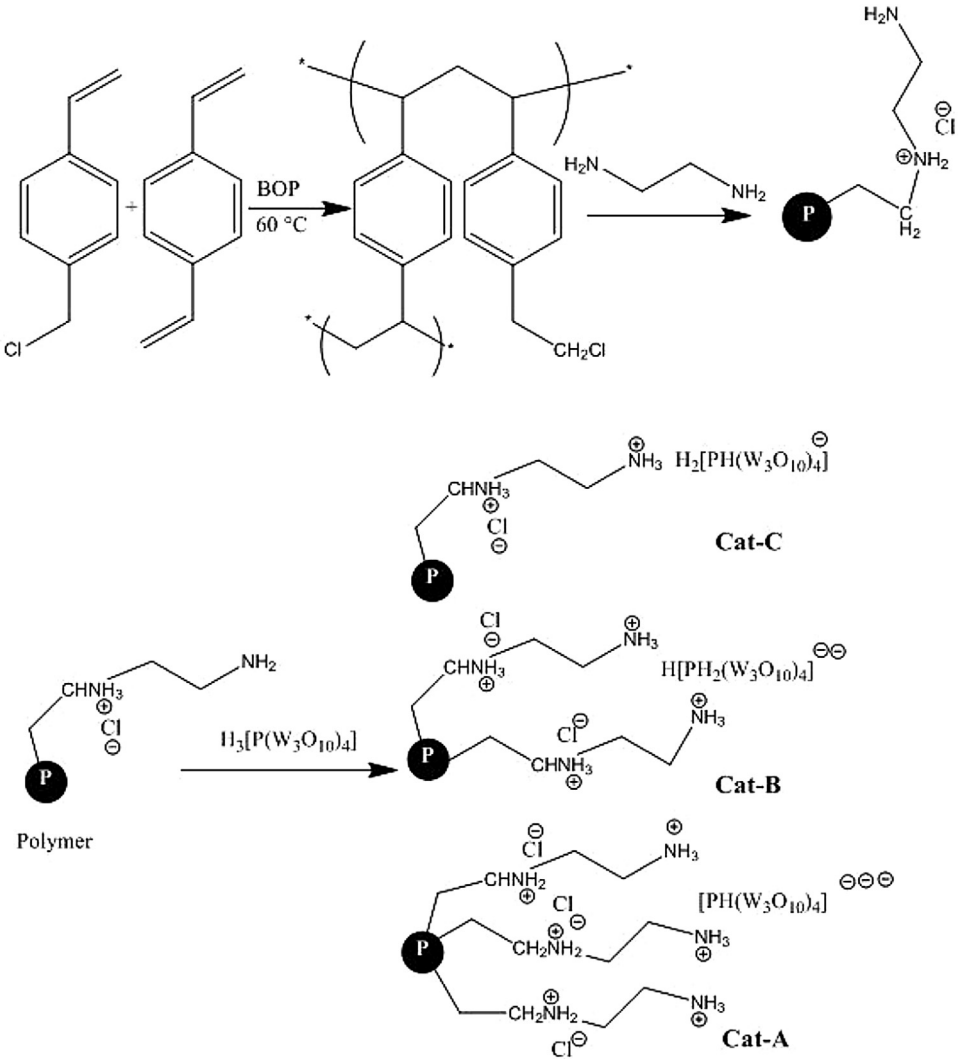

Scheme 1. Preparation of PDVC, H_2N-PDVC and Cat-A, B & C materials.

2.5. Characterization

Field emission scanning electron microscopy (FESEM) and Dispersive X-ray analysis for elemental mapping (FESEM-EDS) were obtained on Zeiss Leo Supra55 microscope. HRTEM analysis was obtained using JEM-2100F. The samples were sonicated for 20 min before the imaging process. XRD patterns were obtained using PANalytical X'Pert PRO diffractometer in reflection mode using CuKα ((λ = 0.1542 nm) at 40 mA and 45 kV. The diffractograms were recorded in the 2θ range of 4–80° with a 2θ step size of 0.01° and a step time of 10 s. FT-IR spectra of samples pressed with dried KBr into discs were recorded on a Nicolet iS10 Spectrometer. Raman scattering spectra analyses were recorded on SENTERRA Dispersive Raman Microscope (Bruker) equipped with a diode Nd:YAG laser and a wavelength of 532 nm from frequencies of 500–2000 cm^{-1}. The BET surface area measurements were carried out in a NOVA 3200 system instrument by nitrogen adsorption at 77 K. The samples were outgassed for 3 h at 150 °C under vacuum in the degas port of the adsorption analyzer. The specific surface area was calculated using the Brunauer–Emmett–Teller (BET) model. The pore size distributions were obtained from the adsorption branch of the nitrogen isotherms by the Barrett–Joyner–Halenda (BJH) method. The XPS spectra were recorded on a Thermo Scientific K-ALPHA USA instrument equipped with a dual X-ray source, using the AlKα radiation anode and a hemispherical energy analyzer. analysis were carried out at pass energy (93.90 eV) to ensure enough sensitivity for the acquisition scan, and pass energy (23.50 eV) was used for the scanning of the narrow spectra of W 4f, O 1s, N 1s and C 1s to ensure sufficient resolution.

2.5.1. Determination of VBC in PDVC

The VBC in PDVC was experimentally determined by using titration method [21], in which the strong base anion exchange resin has greater affinity for more highly charged anions over lower-charged ones. Thus, the PDVC was reacted with excess of triethylamine in toluene solution at 80 °C for 16 h, and the solid was filtered off and dried under vacuum for 24 h. Theoretical VBC was calculated based on 100% conversion of VBC to quaternary ammonium salt. PDVC-triethylamonium chloride (1.0 g) was immersed in known volume of potassium hydroxide (100 mmol L^{-1}) for 36 h; causing K^+ ions replace the Cl^- ions of triethylammonium group. After filtration, the filtrate was normalized with HCl (100 mmol L^{-1}) using a titronic electronic burette and phenolphthalein as indicator. The milliequivalent of VBC in polymer was calculated as hydroxide per gram of dry polymer according to the following equation:

$$\text{VBC}(\text{mmol g}^{-1}) = \frac{M_{b(\text{HCl})} - M_{a(\text{HCl})}}{m_{\text{VBC}}}$$

; where M_b and $M_{a(\text{HCl})}$ are millimoles of HCl determined before and after neutralization, and m_{VBC} is the dry mass (g) of PDVC- triethylamonium in the hydroxide form. The measured VBC on PDVC material is of 3.55 mmol g^{-1}.

2.5.2. Determination of acidity for the prepared catalysts

The total surface acidity for prepared catalysts was determined by *n*-butylamine titration [22]. A 0.1 g of PTA-H_2N-PDVC-x was added to 2.5 mmol L^{-1} of *n*-butylamine in toluene under stirring for 24 h. The excess *n*-butylamine was titrated against trichloroacetic acid using neutral red as an indicator. The measured acidity of Cat-A, Cat-B and Cat-C catalysts is of 2.21, 3.81 & 6.78 mmol g^{-1}, respectively.

2.6. Catalyst Testing

The catalytic acetylation of Gly with AA over Cat-A, Cat-B and Cat-C was performed in a stainless steel autoclave reactor (Parr 4848, internal volume: 450 cm^3), which was equipped with a magnetic stirrer as well as temperature measurement systems under autogenous pressure and nitrogen atmosphere. The glycerol and required weight of catalyst were first introduced, and then the autoclave was sealed and heated with a fixed heating rate at the desired temperature. After that, acetic acid was pumped into the autoclave at stirring speed of 600 rpm. The total volume of the reactants was kept constant at 200 cm^3. The MAG, DAG and TAG products were studied by varying the reaction parameters such as reaction temperature, molar ratio (MR) of the reactants and catalyst weight. After the stipulated reaction time, the product collected through a deep pipe that reached down to the bottom of the autoclave afterwards being let out by a discharge valve to a system of receivers then filtered to separate the catalyst. Agilent 7820A GC equipped with a capillary column (DB-5, 30 m × 0.25 mm i.d., film thickness 0.20 mm) was used to analyze the products. An internal standard as n-hexadecane was used to calculate reaction conversions. The conversion of glycerol and selectivity of products were calculated on the basis of the following equations:

$$\text{Conv.}(\%) = \frac{\text{Amount of glycerol converted}}{\text{Total amount of feeded glycerol}} \times 100$$

$$\text{select.}(\%) = \frac{\text{Amount of glycerol converted to a product}}{\text{total amount of glycerol converted}} \times 100$$

3. Results and discussion

One of the most promising approaches is to design high acidic heterogeneous–homogeneous catalyst containing $H_3[P(W_3O_{10})_4]^-$ as active acidic moieties based on easy separating and recovering from the product mixture. Scheme 1 shows the procedures for the amine surface modification of PDVC and immobilization of $H_3[P(W_3O_{10})_4]$ onto the surface and pore of NH_2-PDVC materials. The surface modification of PDVC was achieved by reacting the chloromethyl group of the VBC with one-NH_2 group of ED under nitrogen atmosphere and immobilization of PTA on the second ED amine group through strong driving force, polymer-$CH_2N^+Cl^-C_2H_4$-$NH_3H_2[P(W_3O_{10})_4]$. Moreover, PTA can be interacted with polymer-$CH_2N^+Cl^-C_2H_2$-$NH_3H_2[P(W_3O_{10})_4]$ to give polymer-$CH_2N^+[H_2[P(W_3O_{10})_4]^-]_2$ and hydrochloric acid.

Fig. 1 shows FTIR of the PDVC, H_2N-PDVC and Cat-A, B&C materials. The PDVC and H_2N-PDVC show bands at 3023, 2926, 2857, 1608, 1515, 1450, 1260 and 753 cm^{-1} that can be attributed to C—H, CH_2 , C—H, —C=C— (Benzene ring), C—H_2 , C—Cl, C—H stretching and C—H bending, respectively. The disappearance of the band at 1260 cm^{-1} attributed to the CH_2Cl group along with the appearance of the new bands at 1404 cm^{-1} attributable to the C—N vibration, showing that effective interaction between ED and CH_2Cl group has occurred. In addition, the formation of a wide broad band between 3341 and 3664 cm^{-1} is due to the vibrations of N—H bonds in —NH_3 group and H—OH, respectively [23,24]. These —OH groups provide the

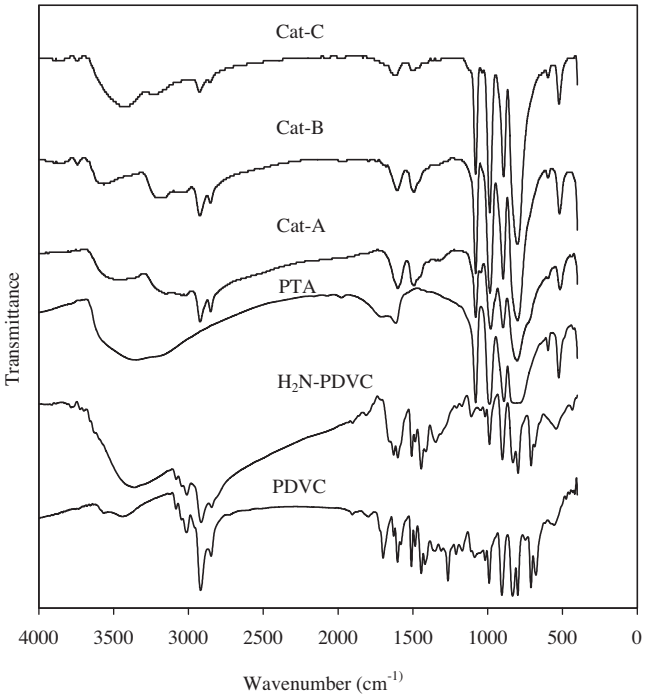

Fig. 1. FTIR spectra of PDVC, H_2N-PDVC, PTA and Cat-A, B & C materials.

sites of hydrogen bonding between onium salt or PTA and water, because the onium salt and PTA were observed to retain water, even at high temperatures. The unsupported PTA shows four characteristic bands appearing at 1084, 985, 906 and 822 cm^{-1} that are assigned to central tetrahedral PO_4 (P—O), stretching modes of the terminal W=O, edge sharing of W—O_b—W and corner sharing W—Oc—W units, respectively. The characteristic bands of Cat-A, B & C show the same bands of the unsupported PTA. However, W—O and W—O—W bands of $[PW_{12}O_{40}]^{3-}$ in the Cat-A, B&C samples appeared at slightly red-shift positions compared to those of the unsupported one, indicating the presence of a strong interaction between $[PW_{12}O_{40}]^{3-}$ and H_2N-PDVC material [25]. In addition, the new absorption band at 1503 cm^{-1} appeared, indicating the weak π-bond interaction of aromatic resin structure with PTA moiety.

The PTA and Cat-A, B & C catalysts were characterized by Raman spectroscopy, as shown in Fig. 2. Following Bridgman's assignments [26], the peaks at 93, 154, 222 cm^{-1} are assigned to O—W—O_t (O_t = terminal oxygen), ν_s(W—O—W) and (W—O_m) (O_m = oxygen in bridge or m-oxo) [27], while the peak at 541 cm^{-1} is corresponded to δ(W—O—W), δ(O—P—O) of phosphotungstate anion. The peak at 928 cm^{-1} assigned asymmetric ν_{as}(W—O_t) and ν_{as}(W—O—W), and the strong peak at 1011 cm^{-1} (ν_s(W—O—W)) is characteristic of highly condensed polymeric phosphotungstate with Keggin structure. In Fig. 2, for Cat-A, B catalysts, the Raman bands intensity at 1011 cm^{-1} is decreased, indicating high dispersion of isolated PTA species. This finding suggests that the PTA species are finely and molecularly dispersed on the surface of NH_2-PDVC. Moreover, the Raman spectrum of Cat-C is somewhat comparable to that of the bulk PTA, indicating that the PTA species over Cat-C shows some characteristics of bulk PTA. Consequently, the PTA species may be well dispersed on the NH_2-PDVC support due to selective impregnation, however PTA was overcrowded on H_2N-PDVC catalyst due to the shorten chain length of ED.

Fig. 3 shows the XRD patterns of bulk PTA and Cat-A, B & C. The bulk PTA shows the typical pattern of Keggin anion construction. On the other hand, the PDVC sample showed no characteristic XRD pattern due to the amorphous nature of PDVC material whereas a new peak at 2θ of 26.6° after amination appeared. It is interesting

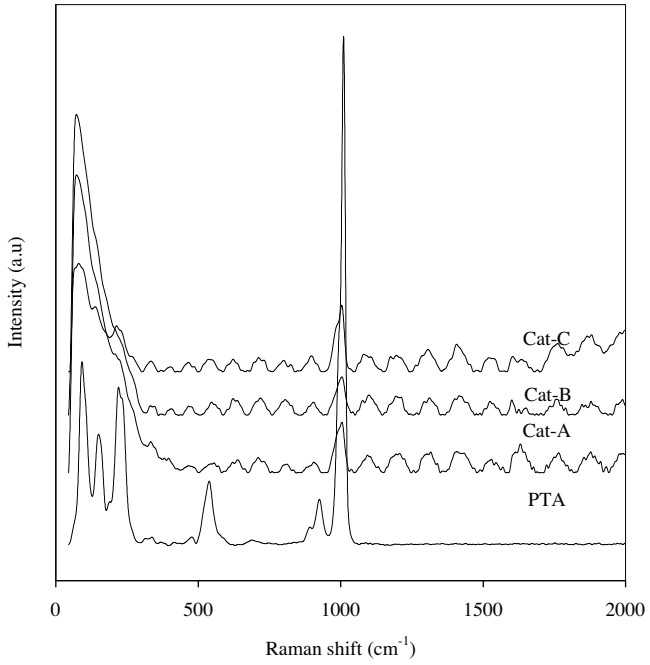

Fig. 2. Raman spectra of the PTA and Cat-A, B & C materials.

that the reaction of PTA with $-NH_2$ of PDVC showed new peaks in region $4^\circ < 2\theta < 9^\circ$, around the plane (1 1 0) due to accommodate to PTA protons onto NH_2-PDVC [28]. The Cat-A showed disappearance of main characteristic peak of PTA at 2θ of 26°, which indicating that the PTA species were not in a crystalline state but are finely and molecularly dispersed on the surface of NH_2-PDVC material. The XRD of Cat-B & C showed typical peaks related to Keggin structure except the peak attributed to NH_2-PDVC that shifted toward high angle, 26.9°. However, the intensity of peaks related to Cat-B & C is reduced, mainly due to parity matching between the PTA and $-NH_2$ moieties, which are located on and inside the pores of NH_2-PDVC, indicating that PTA was chemically attached and semidispersed on NH_2-PDVC.

Fig. 4 shows the surface composition and chemical states of PDVC, H_2N-PDVC and Cat-C materials. The survey spectrum XPS showed that the materials were composed of the elements of C, N, O, Cl, P and W (Fig. 4a). As shown in Fig. 4b, the C1s peak at BE (binding energy) of 284.6 eV is assigned to the CH (—CH═CH—, phenyl). The two additional peaks appeared at 284.8 and 286.4 eV can ascribed to the contributions of C—C skeletal backbone and C—Cl bond. The $[CH_2Cl]/[CH+CH_2]$ area ratio of about 47.5 is slightly above the theoretical ration of divinylbenzene and vinylbenzyl chloride of ~46.6 dictated by PDVC chemical structure, indicating most of VBC located at the surface of PDVC. Fig. 4c shows the XPS spectra of H_2N-PDVC materials. The N 1s region can be deconvoluted into two components. The peak component at about 399.1 eV is assigned to amine ($-NH_2$) moiety of the ED, whereas the peak at about 402.4 eV is assigned to the $-N^+$ (ammonium ions) [29], indicating quaternization of one endcapped amine group. After reaction between H_2N-PDVC and PTA, this peak is completely shifted to 402.6 eV due to existence the electrostatic/ionic interaction and hydrogen bonding interaction between PTA and amine groups of H_2N-PDVC material (Fig. 4g). As illustrated in Fig. 4e, the C1s core level spectra of Cat-C could be deconvoluted into two chemically different components at 288.1 and 285.2 eV. The higher BE component observed at 288.4 eV can be assigned to the C—N^+ and 285.6 eV BE peak is attributed to the CC present in ED bound to PTA, indicating the successful reaction of PTA and free $-NH_2$ of the polymer. The Cl 2p spectrum of H_2N-PDVC and Cat-C showed a peak near 200.2 eV assigned to negatively charged chloride ion, supporting that the bonds between chlorine and nitrogen are ionic (Fig. 4c and f). The high-resolution spectrum showed that BE of 533.7 eV, which assigned to O 1s (Fig. 4h). The BE of 137.3 eV is ascribed to P 2p, which was shifted to high BE by 1.3 eV in comparison with bulk PTA (136.0 eV) [30] implying bond formation between PTA and H_2N-PDVC (Fig. 4i). The W 4f XPS spectrum of Cat-C showed two BE at 36.68 and 38.78 eV, which was attributed to $W4f_{7/2}$ and $W4f_{5/2}$, respectively. In general, bulk PTA showed two BE of 35.8 and 37.9 eV [30]. Compared with the BE values of the bulk PTA, 0.88 eV of BE was shifted to higher BE, indicating that W═O bond was changed to W—O— bond due to the chemical interaction with $-NH_2$ groups of the polymer [31].

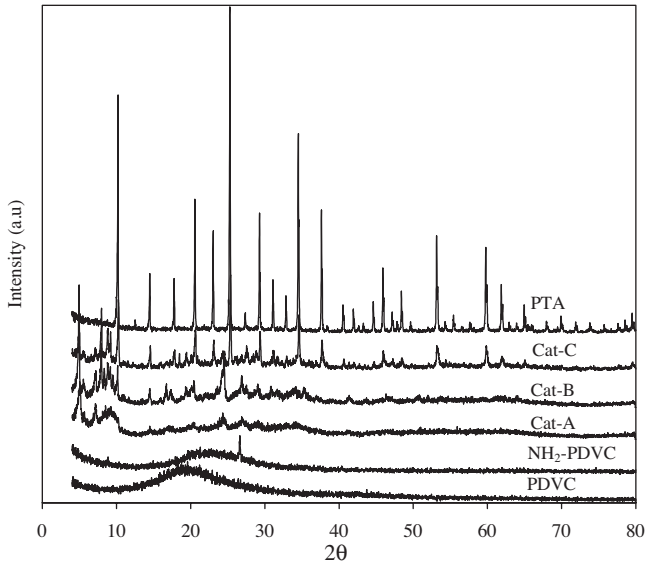

Fig. 3. XRD patterns of pure PDVC, NH_2-PDVC and Cat-A, B & C materials.

Fig. 5 shows RHTEM images of the PDVC, H_2N-PDVC and Cat-A, B & C materials. The TEM image of the PDVC shows that the particles have ropes morphology connected to each other, forming irregular pores with a size of 15–80 nm (Fig. 5a), whereas the pinned ropes became finer, and the pendant methylene groups appear filled the pores after quaternization (Fig. 5b). After reaction with PTA, the ropes became more overlapped due to attachment of more amine site of different rope to one PTA molecule in Cat-A (Fig. 5c). With increasing PTA ratio, the ropes appeared thicker without aggregation for Cat-B (Fig. 5d), however Cat-C showed that the surface was coarser than other samples, and the pores were almost invisible. This result demonstrates that the PTA molecule is in multilayer over PDVC ropes (Fig. 5d).

Fig. 5f presents FESEM image of PDVC, showing asymmetric microspheres morphology with mean diameter particles of 6.6 μm. The FESEM image of Cat-A (Fig. 5g) shows microspheres cluster with asymmetric coalesce with average diameter of ~62 μm, suggesting that PTA protonates different $-NH_2$ groups of more microsphere. However, with increasing PTA loading (Cat-C), the asymmetric microspheres are completely coated with PTA material (Fig. 5h).

The specific surface areas and pore size distribution of the PDVC, H_2N-PDVC and Cat-A, B & C materials are shown in Fig. 6. The materials show mixed of type-IV and I isotherms with H3 desorption isotherm, which demonstrating the existence of micro- and mesopores in these materials. Type H3 hysteresis is usually found on solids with a very wide distribution of pore size. The isotherms for all samples start at low partial pressure, indicating the presence of framework microporosity, whereas the second sharpness at a

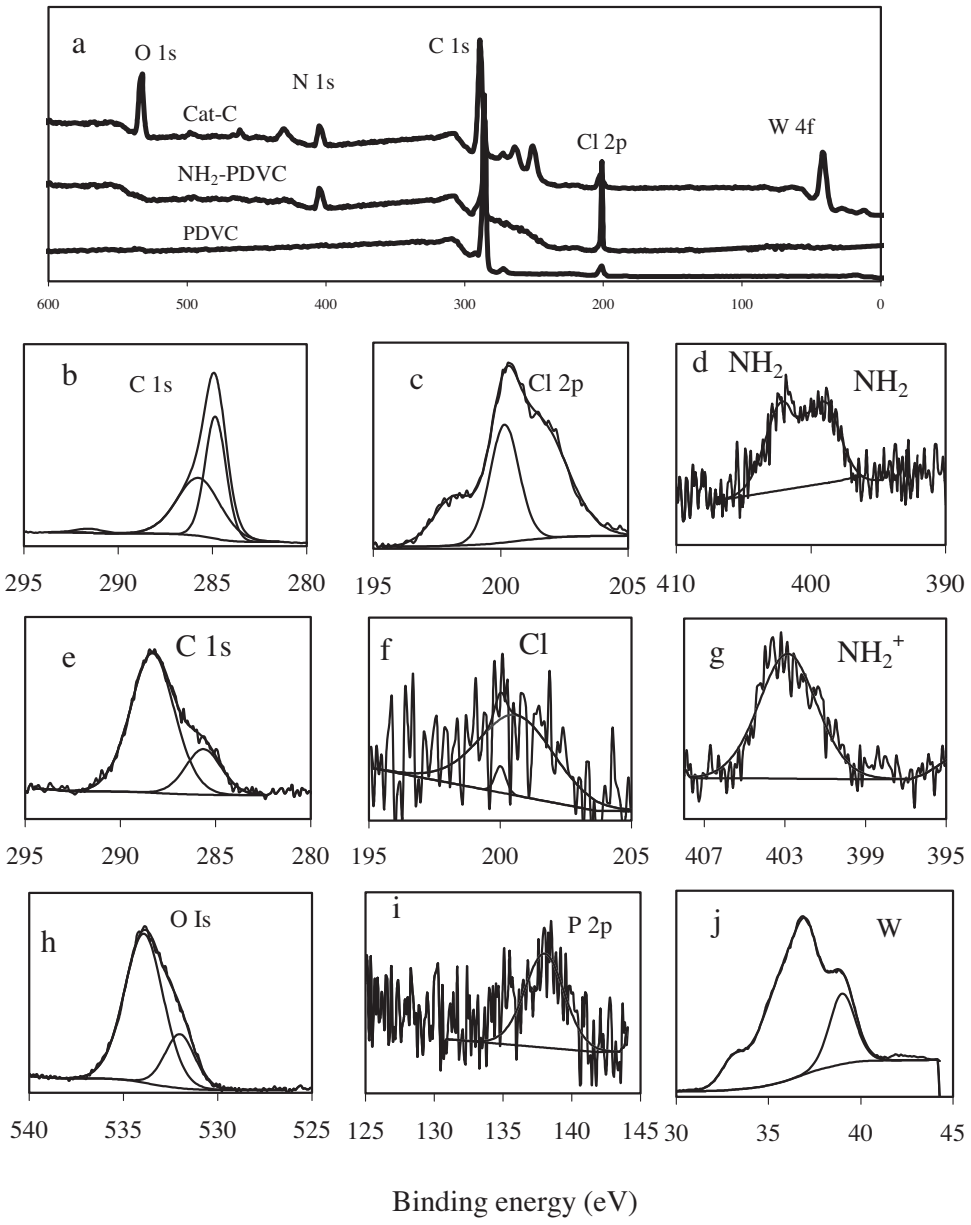

Fig. 4. XPS spectra of (a) Wide scan of C 1s, Cl 2p, N 1s, O 1s, P 2p and W 4f. (b and c) C 1s, Cl 2p of PDVC. (d) N 1s of H_2N-PDVC. (e–j) C 1s, Cl 2p, N 1s, O 1s, P 2p and W 4f of Cat-C.

partial pressure of about 0.83–0.97 is due to the textural interparticle pores [32]. Compared with the bare PDVC, the H_2N-PDVC and Cat-A, B & C exhibit a significant decrease of surface area, indicating that the cavities of PDVC are presumably occupied by $-NH_2$ and PTA–N^+H_3 particles. After the loading of PTA, the surface area of PDVC (673 $m^2\,g^{-1}$) significantly decreases to 367, 205, 141 and 65 $m^2\,g^{-1}$ for H_2N-PDVC and Cat-A, B & C, respectively. All the samples present multi and broad pore size distributions. The PDVC shows multipore size in mesoporous range at 2.4, 3.4 and 4.9 nm, however these pores shifted to lower values and new pore after grafting PTA material appeared. The Cat-A shows a new pore size at 8.0 nm indicating further formation of a new pore resulted from

Table 1
Gly conversion and product selectivities to MAG, DAG and TAG in the acetylation of Gly with AA catalyzed by various materials. Catalyst weight (4%), run time (3 h) and Gly/AA ratio (1:6)

Catalysts	60 °C				80 °C				100 °C			
	Con.	MAG	DAG	TAG	Con.	MAG	DAG	TAG	Con.	MAG	DAG	TAG
Blank	4.5	100	0	0	11	100	0	0	16	96	4	0
NH_2-PDVC	15	100	0	0	23	98	2	0	28	93	7	0
Cat-A	55	74.6	18.4	7	63	37	55	8	73	25.3	56	18.7
Cat-B	62	65	24	11	75	31	45	24	91	10.7	46.7	42.6
Cat-C	76	47	35	18	93	22	44	34	99	3.3	41.3	55.4

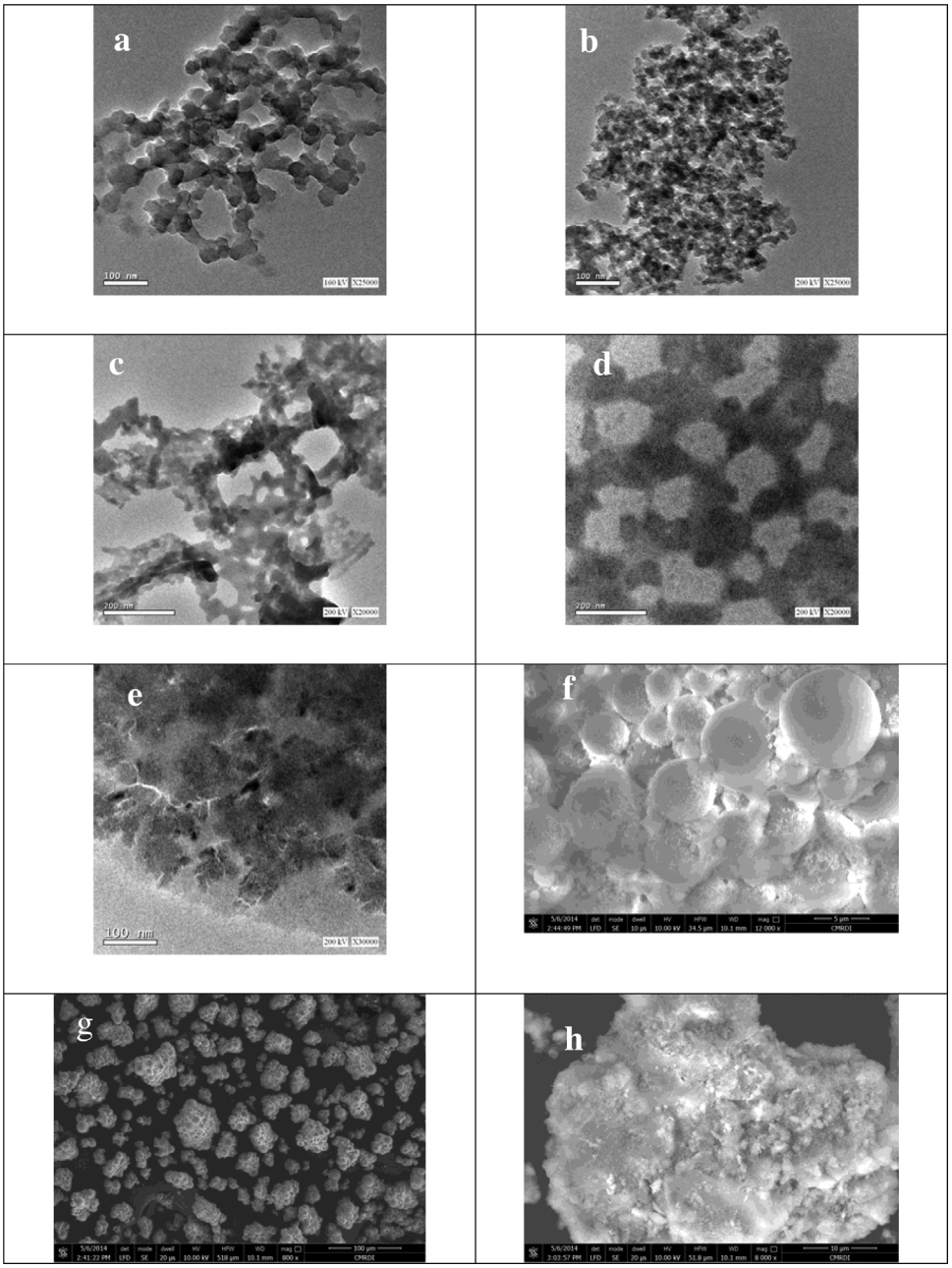

Fig. 5. HRTEM images of (a) PDVC, (b) H_2N-PDVC and (c-e) Cat-A,B&C materials, and FESEM of (f)PDVC, (h) Cat-A and (g) Cat-C materials.

crosslinking of PTA and more $-NH_2$ of different particles. This peak value is gradually decreases and became broad with increase in PTA loading due to repulsion between PTA anions, while the other peaks of the PDVC material is diminished because of PTA is compacted on the PDVC surface.

3.1. Catalytic activity

The catalytic activity of H_2N-PDVC and Cat-A, B & C materials was evaluated in the acetylation reaction of Gly with AA. Screening of the reaction parameters including temperature, Gly/AA MR, catalyst weight and reaction time was made, and the acetylation reaction was also performed in the absence of the catalyst at the same conditions. During esterification process of Gly with AA, one or more hydroxyl groups in the Gly molecule react with AA. Therefore, depending on the extent of esterification, up to three esters may be formed, MAG, DAG and TAG (Scheme 2).

The influence of temperature on the Gly acetylation over the prepared catalysts was studied at constant Gly/AA MR of 1:6, catalyst weight of 4% and the autoclave temperature adjusted at 60, 80 and 100 °C for 3 h. Table 1 shows that the Gly conversion and selectivity to TAG increase with increasing temperatures. The reaction proceeds even in the absence of a catalyst, since presence of excess acetic acid promotes the acidity of the reaction medium, reaching 4.5, 11 and 16% at temperatures of 60, 80 and 100 °C, respectively. Moreover, as listed in Table 1, NH_2-PDVC as a catalyst showed Gly conversion of 15, 23 and 28% with high selectivity of MAG at 60, 80 and 100 °C, respectively. These results may imply that the catalytic performance of amine-anchored polymer catalyst towards the acetylation reaction is dependent on the basicity of the catalyst. It is also suggested that both the free amino group of ED and the

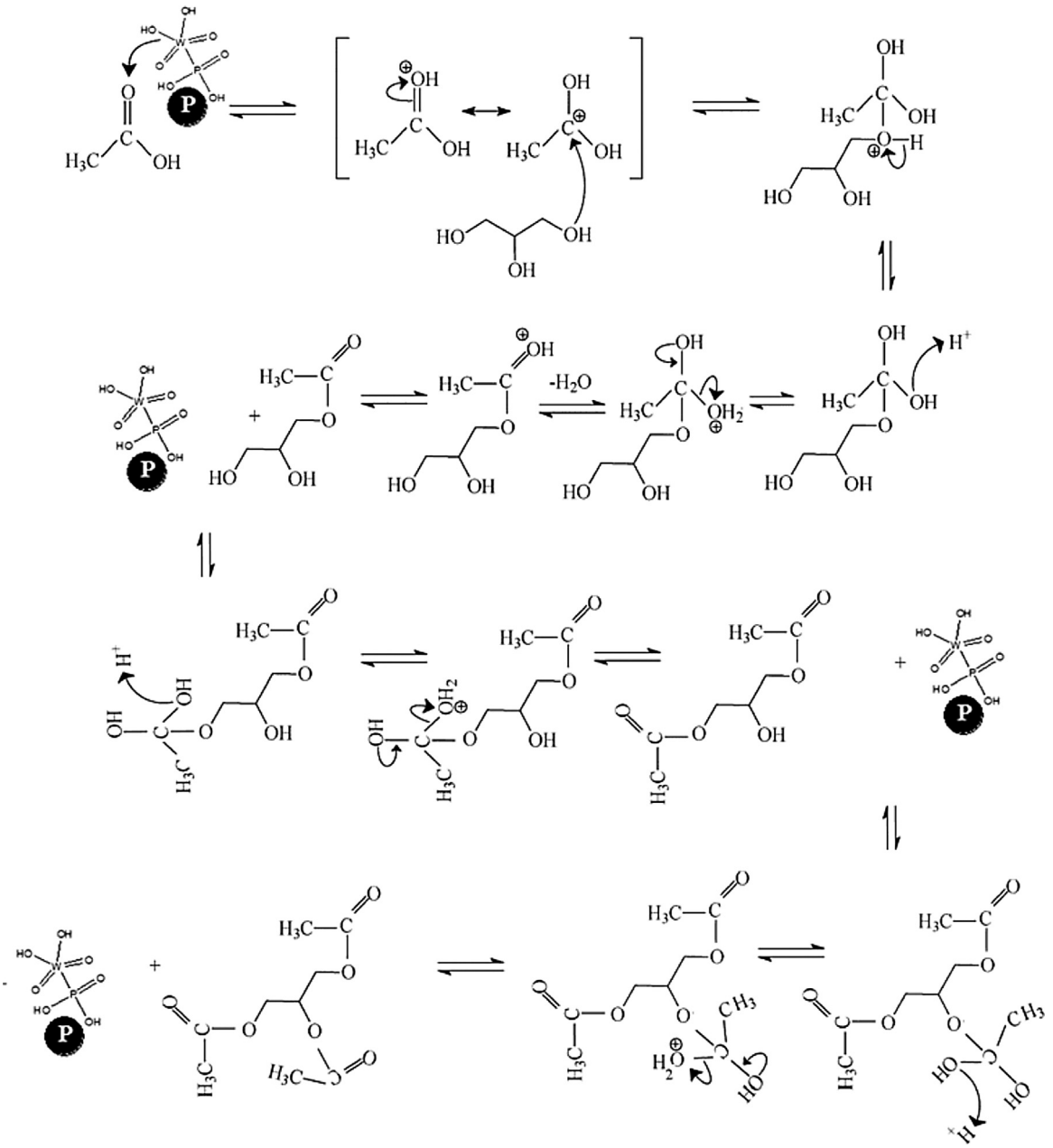

Scheme 2. Mechanism of MAG, DAG and TAG production catalyzed by Cat-C.

chloride anion of amine cation could play catalytic roles, possibly in a cooperative mode [33].

The Cat-A showed Gly conversion reached 55, 63 and 73% at temperatures of 60, 80 and 100 °C, and the MAG was the major product (up to 74.6% selectivity at 60 °C), while DAG was of ≈55% at 80 and 100 °C, respectively. Because of the consecutive acetylation reaction is highly endothermic with temperature-dependent selectivity, the MAG product is the major at low temperature [34]. Moreover, the Gly conversion is of 62, 75 and 91% for Cat-B, and 76, 93 and 99% for Cat-C at 60, 80 and 100 °C, respectively. However, the DAG and TAG selectivities increased with the increasing amount of PTA attached to amine-functionalized polymer. This effect can be explained by the presence of more PTA anions on the surface, which increases the Brønsted acidity of the catalyst and hence enhances the interactions between the acylium moiety of the acetic acid and the OH^- anion of Gly [34]. The selectivity for MAG was high at beginning of the reaction; as the reaction proceeds, the selectivity toward DAG and TAG increased at the consuming of MAG [35]. This behavior can be explained by the formation of acylium ion intermediate by ionic attack of Gly hydroxyl group on acetic acid carbonyl group. Lilja et al. [36] reported that the rate of acylium ion formation on the catalyst acid sites represents the determining step during the acetylation process. The acylium-acid site complex can be subject to multiple nucleophilic attacks of the Gly hydroxyl groups. Indeed, the Gly conversion (blank test) was of 16% with high selectivity for MAG (96%) at 100 °C. However, in the system catalyzed by Cat-C, the Gly conversion favors consecutive reactions with high selectivity for DAG and TAG in all the studied temperatures. Consequently, the DAG and TAG products can be certified to the protonation of the carbonyl oxygen atom of acetic acid and subsequent nucleophilic attack by MAG product (Scheme 2).

It is established that the acetylation process is more favorable to be carried out under excessive AA rather than Gly due to high Gly conversion may not be reached under excessive Gly [37]. From

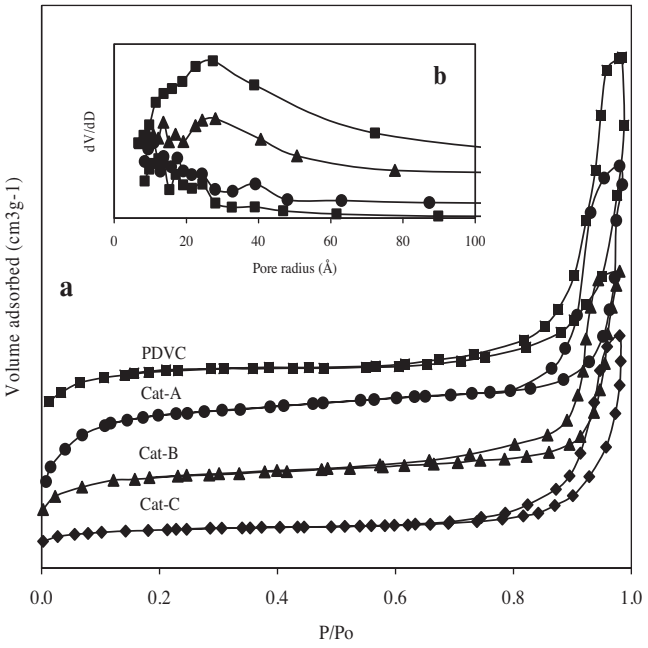

Fig. 6. (a) Nitrogen adsorption–desorption isotherms and (b) the corresponding pore size distribution for various samples.

an economic point of view, TAG prepared near Gly to AA ratio (1:3 MR) hold great economic and considered to be the optimum for saving energy in recovery of excess AA as well as products separation and purification. The acetylation reaction was studied with MR of Gly to AA varying between 1:4, 1:6 and 1:8 at catalyst loading (4%), T (100 °C) and reaction time (3 h). Fig. 7 showed the conversion and the products distribution of Gly over Cat-C as the most active catalyst. It could be seen that Cat-C presented the high conversion of Gly as well as the high selectivity for DAG and TAG at 1:8 molar ratio due to increased availability of acetic acid in the reaction medium, shifting of the product distribution towards higher substituted products. At reaction time of 30 min, the observed glycerol conversion was ~67, 73 and 81% with 1:4, 1:6 and 1:8 MR, respectively. Afterward, the glycerol conversion and selectivity toward the TAG increases enormously with time. A maximum selectivity for TAG was achieved 61.2% at 1:8 molar ratio after 3 h of reaction time, attributed to the consecutive esterification of MAG and DAG to TAG. As well, the Gly acetylation reaction rate increases in the order 1:8 > 1:6 > 1:4, indicating the reactant mixture was the main factor, which had significant influence on the equilibrium time of the products distribution. These results may be due to the excess of acetic acid being able to swell Cat-C, at which Cat-C participates as heterogeneous-homogeneous catalyst. Zhou et al. [38] reported that higher AA to Gly MR facilitatesthe shift of the distribution of the esters towards higher substituted species, and thus higher glycerol conversion and selectivity for DAG and TAG could be achieved. Agnieszka et al. [39] studied the effect of Gly to AA molar ratio on Starbon®-400-SO_3H catalyst. They found that the formation of MAG was favored at short time and lower AA to Gly MR (1:1), whilst the higher MR would favor the formation of DAG and TAG [39], which is in good agreement with our results.

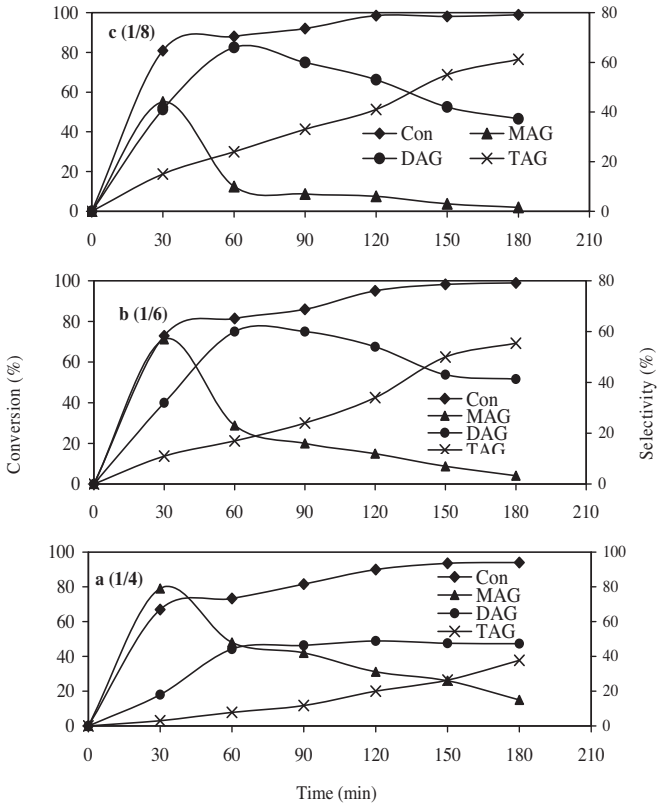

Fig. 7. The products distribution of glycerol acetylation at Gly/AA MR of 1:4, 1:6 and 1:8 at temperatures 100 °C and catalyst weight of 4%.

The influence of the catalyst loading (catalyst-to-Gly) was investigated at 100 °C, Gly to AA (1:8) after reaction time (3 h) over Cat-C in order to courage the formation of TAG. As shown in Fig. 8, the increase of the catalyst loading from 2 to 8 wt% leads to a remarkable increase of TAG selectivity. About 99.9% glycerol conversion with 26.5% DAG and 73% TAG is obtained over 8 wt% catalyst, indicating the selectivity toward TAG increased with increasing the number of available active sites. Ferreira et al. [40], also recorded a similar result on the glycerol acetylation over dodecatungstophosphoric acid immobilized into a silica matrix.

The leaching test of PTA from Cat-C was performed according to the method proposed by Sheldon et al. [41]. After 30 min, the catalyst is collected and reaction medium is analyzed, resulting conversion of 80.9% and selectivities of 44% (MAG), 41.2% (DAG) and 15.3% (TAG). Keeping the reaction condition constant, a new quantification was carried out after 3 h of reaction without catalyst (Fig. 9a). The conversion was of 81.2% and the values of selectivity for DAG and TAG are remained constant, indicating that no PTA is leached. The XRD patterns of Cat-C (Fig. 9b) for recycled catalyst in the glycerol acetylation is similar to fresh Cat-C (Fig. 3). This similarity suggested that the structure of recycled catalyst is preserved and it is stable since catalytic recycling.

Because of the stability of the tested catalyst during reaction is one of the important factors, recycled catalyst tests were conducted. The catalysts were separated from the reaction mixture by filtration, washed with water/methanol (90:10; v/v) several times to remove the un-reacted acetic acid, and vacuum drying before being reused. The Gly conversion and selectivity to MAG, DAG and

Table 2
Influence of the catalyst recycling on conversion and products selectivity in glycerol acetylation reactions over Cat-C catalyst. Catalyst weight (8%), run time (3 h) and Gly/AA ratio (1/8).

Run	Con.	MAG	DAG	TAG
1st	99.90	0.50	26.50	73.00
2nd	99.78	0.55	26.90	72.55
3rd	99.74	0.65	27.25	72.10
4th	99.72	0.82	30.10	69.08
5th	99.71	1.30	31.30	67.40
6th	99.65	1.70	32.80	65.50
7th	99.61	1.77	34.20	64.03

Table 3
Comparison of Cat-C with other reported catalysts for glycerol acetylation reaction

Catalyst	Conditions			Con. (%)	Selectivity (%)			Ref.
	Time (h)	Temp (°C)	Gly:AA		MAG	DAG	TAG	
Amberlyst-15	12	105	1:8	95.6	70.3	4.5	–	[42]
Amberlyst-35	4	105	1:6	99.0	49.1	25.0	25.9	[43]
PTA-AC	3	120	1:16	86.0	25.0	63.0	11	[40]
PTA/Silica	7	120	1:16	87.0	36.0	59.0	4	[44]
PMo_3-USY	3	120	1:18	68.0	37.0	59.0	2	[45]
SZ	24	55	1:8	54.0	98.9	1.2	–	[46]
KJ-400	4	120	1:5	88.5	56.0	40	4	[47]

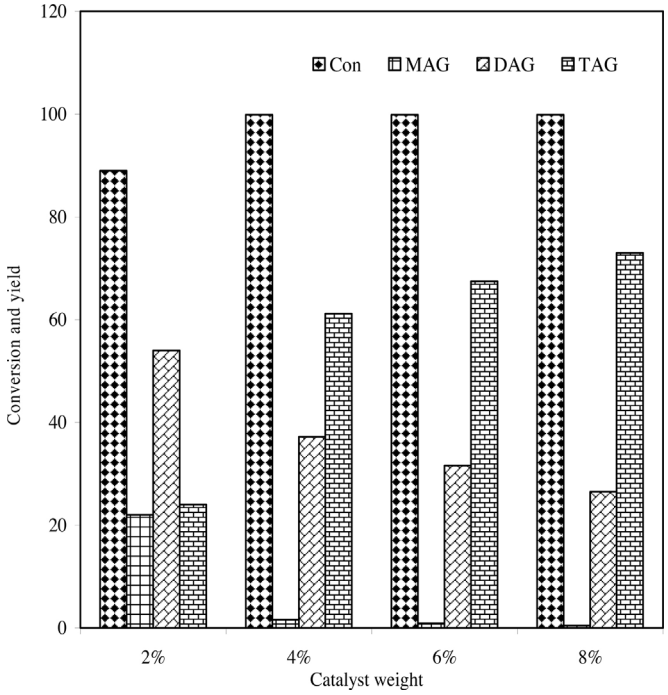

Fig. 8. Influence of the catalyst weight on conversion and products selectivity in glycerol acetylation reactions over Cat-C; temperature (100 °C), Gly/AA (1:8) and reaction time of 3 h.

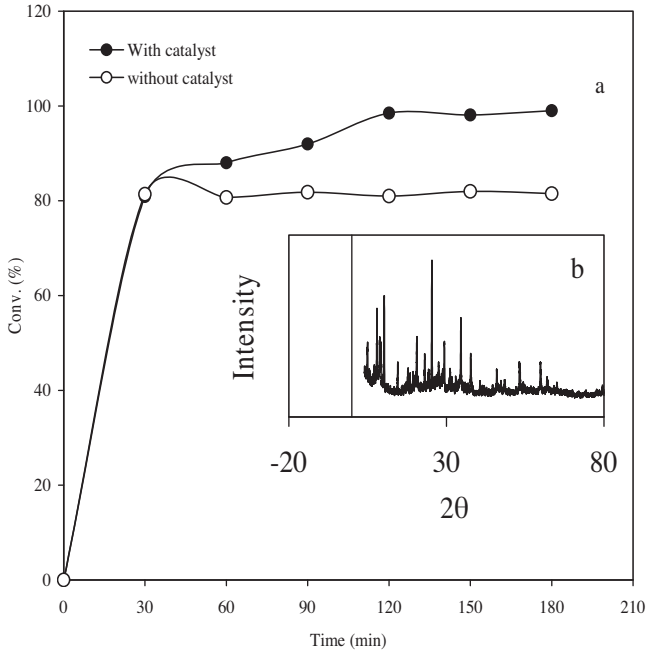

Fig. 9. (a) The leaching test of PTA from Cat-C; temperature (100 °C), Gly:AA (1:8) and reaction time of 3 h. (b) XRD patterns of used Cat-C catalyst after 7th run.

TAG after six runs are presented in Table 2. The catalyst conversion was of ≈99.7% for all runs, indicating that the catalyst did not undergo any acid leaching during the reactions, whereas the selectivity to MAG and DAG slightly increased to 1.27 and 7.7%, respectively at the expense of TAG form the first to seventh runs. These changes may be due to the loss of catalyst powder during the recycling processes or deactivation of some of acid sites, which leads to the stepwise termination of the contribution of acid sites located inside catalyst.

The activity of Cat-C for glycerol acetylation is compared with other reported solid catalysts and the data was tabulated in Table 3. It could be seen that Amberlyst-15&35, PTA/active carbon, PTA/silica and KJ-400 (biochar carbon) showed high activity as well as noticeable selectivity for DAG and TAG compared to dodecamolybdophosphoric acid/USY-zeolite and sulfated zirconia catalyst (SZ). However, the remarkable activity of Cat-C may be due to two reasons: firstly, Cat-C has high catalytic acid group (PTA) that enhances the formation of the reactive electrophilic intermediate; secondly Cat-C has enough pore space and excellent swelling ability, especially in acetic acid, facilitating the formation of TAG molecule.

4. Conclusions

In summary, the authors developed micro-mesopores H_2N-PDVC polymer and reported the first successful immobilization of catalytically active acidic Keggin-type ($H_3PW_{12}O_{40}$, PTA) material on the surface and pores of H_2N-PDVC framework material. The resulting H_2N-PDVC material is coated with a customized ratio of PTA through an innovative approach that increases the activity, durability and recyclability of the catalyst. PTA-H_2N-PDVC can catalyze the glycerol acetylation with high-excellent efficiency and completely avoiding the formation of by-products because of the special morphology of the catalyst, in which polymer acts as heterogeneous support and PTA attached to ethylenediamine acts as homogenous catalyst.

The efficiency of the acetylation reaction is significantly influenced by the strength of the acidic sites in the H_2N-PDVC material. The obtained catalyst exhibited high activity for glycerol acetylation under mild conditions (T = 100 °C; Gly: AA = 1:8 and time = 3 h) and also showed high selectivity towards TAG (73.0%) than previously described reports. Furthermore, the catalyst is simply recoverable and can be reused 6th times with no leaching or deactivation due to the ionic bonding interaction of PTA with the amine groups of H_2N-PDVC. Consequently, PTA-H_2N-PDVC as a heterogeneous-homogeneous catalyst has great interest for further industrial applications.

References

[1] J. Behr, K. Eilting, J. Irawadi, F. Leschinski Lindner, Green Chem. 10 (2008) 13–30.
[2] A. Sakthivel, R. Nakamura, K. Komura, Y. Sugi, J. Supercrit. Fluids 42 (2007) 219–255.
[3] N. Rahmat, A.Z. Abdullah, A.R. Mohamed, Renew. Sustain. Energy Rev. 14 (2010) 987–1000.
[4] T. Miyazawa, S. Koso, K. Kunimori, K. Tomishige, Appl. Catal. A: Gen. 329 (2007) 30–35.
[5] M.A. Dasari, P. Kiatsimkul, W.R. Sutterlin, G.J. Suppes, Appl. Catal. A: Gen. 281 (2005) 225–231.
[6] P. McMorn, G. Roberts, G.J. Hutchings, Catal. Lett. 63 (1999) 193–197.
[7] S. Demirel-Gulen, M. Lucas, P. Claus, Catal. Today 102 (2005) 166–172.
[8] E.P. Maris, R.J. Davis, J. Catal. 249 (2007) 328–337.
[9] H.J. Lee, D. Seung, K.S. Jung, H. Kim, I.N. Filimon, Appl. Catal. A:Gen. 390 (2010) 235–244.
[10] J.A. Melero, R.V. Grieken, G. Morales, M. Paniagua, Energy Fuels 21 (2007) 1782–1791.
[11] V.L.C. Gonçalves, B.P. Pinto, J.C. Silva, C.J.A. Mota, Catal. Today 133–135 (2008) 673–677.
[12] T.S. Galhardo, N. Simone, M. Gonçalves, F.C.A. Figueiredo, D. Mandelli, W.A. Carvalho, ACS Sust. Chem. Eng. 1 (2013) 1381–1389.
[13] M.S. Khayoon, B.H. Hameed, Bioresour. Technol. 102 (2011) 9229–9235.
[14] P. Ferreira, I.M. Fonseca, A.M. Ramos, J. Vital, J.E. Castanheiro, Appl. Catal. B: Environ. 91 (2009) 416–422.
[15] A.C. Garade, V.S. Kshirsagar, R.B. Mane, A.A. Ghalwadkar, U.D. Joshi, C.V. Rode, Appl. Clay Sci. 48 (2010) 164–170.
[16] L. Zhang, Q. Jin, L. Shan, Y. Liu, X. Wang, J. Huang, Appl. Clay Sci. 47 (2010) 229–234.
[17] C.H. Zhou, Appl. Clay Sci. 48 (2010) 1–4.
[18] K. Jagadeeswaraiah, M. Balaraju, P.S. Sai Prasad, N. Lingaiah, Appl. Catal. A: Gen. 386 (2010) 166–170.
[19] S. Singh, A. Patel, Ind. Eng. Chem. Res. 53 (2014) 14592–14600.
[20] M. Balaraju, P. Nikhitha, K. Jagadeeswaraiah, K. Srilatha, P.S. Sai Prasad, N. Lingaiah, Fuel Process. Technol. 91 (2010) 249–253.
[21] L. Dominguez, J. Economy, K. Benak, C.L. Mangun, Polym. Adv. Technol. 14 (2003) 632–637.
[22] H.R. Sahu, G.R. Rao, Bull. Mater. Sci. 23 (2000) 349–354.
[23] A. Akelah, A. Rehab, T. Agag, M. Betiha, J. Appl. Polym. Sci. 103 (2007) 3739–3750.
[24] A. Rehab, A. Akelah, T. Agag, M. Betiha, J. Appl. Polym. Sci. 106 (2007) 3502–3514.
[25] H. Kim, P. Kim, K.Y. Lee, S.H. Yeom, J. Yi, I.K. Song, Catal. Today 111 (2006) 361–365.
[26] A.J. Bridgeman, Chem. Phys. 287 (2003) 55–69.
[27] C. R'Deltcheff, M. Fournier, R. Franck, R. Thouvenot, Inorg. Chem. 22 (1983) 207–216.
[28] J.A. Dias, J.P. Osegovic, R.S. Drago, J. Catal. 183 (1999) 83–90.
[29] L. Cen, K.G. Neoh, E.T. Kang, Langmuir 19 (2003) 10295–10303.
[30] M.S. Akhtar, K.K. Cheralathan, J.M. Chun, O.B. Yang, Electrochim. Acta 53 (2008) 6623–6628.
[31] T. Kumaraguru, A.V. Devi, V. Siddaiah, K. Rajdeo, N.W. Fadnavis, Appl. Catal. A: Gen. 486 (2014) 55–61.
[32] A. Khder, H. Hassan, M.A. Betiha, K.S. Khairou, A.A. Ibrahim, React. Kinet. Mech. Catal. 112 (2014) 61–75.
[33] F.S.H. Simanjuntak, J.S. Choi, G. Lee, H.J. Lee, S.D. Lee, M. Cheong, H.S. Kim, H. Lee, Appl. Catal. B: Environ. 165 (2015) 642–650.
[34] V.L.C. Goncalves, B.P. Pinto, J.C. Silva, C.J.A. Mota, Catal. Today 133–135 (2008) 673–677.
[35] U. Freese, F. Heinrich, F. Roessner, Catal. Today 49 (1999) 237–244.
[36] J. Lilja, J. Wärnå, T. Salmi, L.J. Pettersson, J. Ahlkvist, H. Grénman, M. Rönnholm, D.Y. Murzin, Chem. Eng. J. 115 (2005) 1–12.
[37] M. Huang, X. Han, C. Hung, J. Lin, P. Wu, J. Wu, S. Liu, J. Catal. 320 (2014) 42–51.
[38] L. Zhou, T. Nguyen, A.A. Adesina, Fuel Process. Technol. 104 (2012) 310–318.
[39] M.R. Agnieszka, D.M. Johannes, W.M. Bonny, B.H. Kuipers, B.M. Erne, Chem. A Eur. J. 14 (2008) 2016–2024.
[40] P. Ferreira, I.M. Fonseca, A.M. Ramos, J. Vital, J.E. Castanheiro, Catal. Commun. 12 (2011) 573–576.
[41] R.A. Sheldon, M. Wallau, I.W.C.E. Arends, U. Schuchardt, Acc. Chem. Res. 31 (1997) 485–493.
[42] I. Dosuna-Rodríguez, E.M. Gaigneaux, Catal. Today 195 (2012) 14–21.
[43] X. Liao, Y. Zhu, S. Wang, Y. Li, Fuel Process. Technol. 90 (2009) 988–993.
[44] M. Trejda, K. Stawicka, A. Dubinska, M. Ziolek, Catal. Today 187 (2012) 129–134.
[45] P. Ferreira, I.M. Fonseca, A.M. Ramos, J. Vital, J.E. Castanheiro, Cat. Commun. 10 (2009) 481–484.
[46] I. Dosuna-Rodríguez, C. Adriany, E.M. Gaigneaux, Catal. Today 167 (2011) 56–63.
[47] J.M. Rafi, A. Rajashekar, M. Srinivas, B.V.S.K. Rao, R.B.N. Prasad, N. Lingaiah, RSC Adv. 5 (2015) 44550–44556.